Applied Physics Letters ARTICLE pubs.aip.org/aip/apl

Polarization-induced 2D electron gases in N-polar AlGaN/AlN heterostructures on single-crystal AlN substrates

Cite as: Appl. Phys. Lett. **122**, 212106 (2023); doi: 10.1063/5.0145826
Submitted: 8 February 2023 · Accepted: 8 May 2023 ·
Published Online: 24 May 2023

View Online

Export Citation

CrossMark

Zexuan Zhang,[1,a] Jashan Singhal,[1,b] Shivali Agrawal,[2] Eungkyun Kim,[1] Vladimir Protasenko,[1] Masato Toita,[3] Huili Grace Xing,[1,4,5] and Debdeep Jena[1,4,5]

AFFILIATIONS

[1]School of Electrical and Computer Engineering, Cornell University, Ithaca, New York 14853, USA
[2]School of Chemical and Biomolecular Engineering, Cornell University, Ithaca, New York 14853, USA
[3]Advanced Devices Technology Center, Asahi Kasei Corporation, Hibiya Mitsui Tower, 1-1-2 Yurakucho, Chiyoda-ku, Tokyo 100-8440, Japan
[4]Department of Materials Science and Engineering, Cornell University, Ithaca, New York 14853, USA
[5]Kavli Institute at Cornell for Nanoscale Science, Ithaca, New York 14853, USA

[a]Author to whom correspondence should be addressed: zz523@cornell.edu
[b]Electronic mail: js3452@cornell.edu

ABSTRACT

Polarization-induced carriers play an important role in achieving high electrical conductivity in ultrawide bandgap semiconductor AlGaN, which is essential for various applications ranging from radio frequency and power electronics to deep UV photonics. Despite significant scientific and technological interest, studies on polarization-induced carriers in N-polar AlGaN are rare. We report the observation and properties of polarization-induced two-dimensional electron gases (2DEGs) in N-polar AlGaN/AlN heterostructures on single-crystal AlN substrates by systematically varying the Al content in the 8 nm top layers from $x = 0$ to $x = 0.6$, spanning energy bandgaps from 3.56 to 4.77 eV. The 2DEG density drops monotonically with increasing Al content, from $3.8 \times 10^{13}/\text{cm}^2$ in the GaN channel, down to no measurable conductivity for $x = 0.6$. Alloy scattering limits the 2DEG mobility to below $50\,\text{cm}^2/\text{V s}$ for $x = 0.49$. These results provide valuable insights for designing N-polar AlGaN channel high electron mobility transistors on AlN for extreme electronics at high voltages and high temperatures, and for UV photonic devices.

Published under an exclusive license by AIP Publishing. https://doi.org/10.1063/5.0145826

Highlighted by many figure-of-merits of device performance which scale non-linearly with energy bandgap, ultrawide bandgap (UWBG) semiconductors, such as Ga_2O_3, AlGaN, and diamond, represent an emerging area of research in materials, physics, device, and applications ranging from radio frequency (RF) and power electronics, deep-UV photonics as well as quantum computing and applications under harsh environments.[1,2] AlGaN, possessing a bandgap that can be tuned from 3.4 to over 6 eV by controlling the Al composition in the alloy, has garnered significant research and technological interest as a building block for various electronic and photonic applications.[3–6] In addition to the wide range of energy bandgaps it can cover, AlGaN is the only UWBG material where conductive channels (both p-type and n-type) can be induced by polarization engineering without chemical doping.[7,8]

Unlike in metal-polar AlGaN,[3,4,8–10] reports on polarization-induced electrons in N-polar AlGaN, however, have been limited.[11,12] Analogous to the polarization-induced two-dimensional electron gases (2DEGs) observed at metal-polar $Al_yGa_{1-y}N$/$Al_xGa_{1-x}N$ heterointerfaces ($y > x$),[3,4,9] the positive polarization charge and conduction bandoffset at the heterointerface should also generate a 2DEG in a N-polar AlGaN/AlN heterostructure. Such 2DEGs, despite being largely unstudied, can be used as the channels for N-polar AlGaN channel high electron mobility transistors (HEMTs) on AlN where the absence of top barriers can potentially mitigate the issue of poor electrical contacts faced by their metal-polar counterparts while simultaneously taking advantage of the large breakdown fields of the wide bandgap AlGaN channel and AlN barrier.[11,12]

Published under an exclusive license by AIP Publishing

Downloaded from http://pubs.aip.org/aip/apl/article-pdf/doi/10.1063/5.0145826/17813233/212106_1_5.0145826.pdf

In addition to the energy bandgap of the channel, the properties of 2DEGs in N-polar AlGaN/AlN heterostructures are also expected to be tunable by varying the Al composition in AlGaN.[9] Besides a significant scientific interest in understanding carrier transport in N-polar AlGaN, a systematic study of the compositional dependence of the structural, electrical, and optical properties of N-polar AlGaN/AlN heterostructures is of technological importance as these properties translate directly to the device performance. Moreover, since structural defects are known to affect the properties of a material and degrade device performance,[13–16] it is desirable to explore how N-polar AlGaN/AlN structures on lattice-matched, structurally pure single-crystal AlN substrates with dislocation densities $<10^4/\text{cm}^2$ compare with the commonly used foreign substrates such as SiC or sapphire where the large lattice mismatch between AlN and the substrates leads to high density of dislocations ($\sim10^9/\text{cm}^2$).[11,12,17]

In this work, we investigated the formation and properties of polarization-induced 2DEGs in N-polar $Al_xGa_{1-x}N/Al_{0.85}Ga_{0.15}N$ heterostructures ($x = 0$ to $x = 0.6$) on single-crystal AlN. The thicknesses of the top $Al_xGa_{1-x}N$ and bottom $Al_{0.85}Ga_{0.15}N$ layers are ∼8 and 40 nm, respectively. Optical bandgaps of the top AlGaN layers extracted from photoluminescence (PL) spectra span from 3.56 to 4.77 eV. In addition to a charge control from $n_s = 3.8 \times 10^{13}/\text{cm}^2$ at $x = 0$ to $n_s = 7.6 \times 10^{12}/\text{cm}^2$ at $x = 0.49$ and eventually not measurable when $x = 0.6$, a decrease in electron mobility is observed upon increasing Al content x, from ∼650 ($x = 0$) to ∼40 cm^2/V s ($x = 0.49$) at 300 K, as expected from alloy scattering.

The epitaxial heterostructures shown in Fig. 1(a) were grown using plasma-assisted molecular beam epitaxy (MBE) in a Veeco GEN10 system equipped with standard effusion cells for Ga and Al and a radio frequency plasma source for active N species. Two Al cells were used for the growth of abrupt heterojunctions. KSA Instruments reflection high-energy electron diffraction (RHEED) apparatus with a Staib electron gun operating at 15 kV and 1.5 A was used to *in situ* monitor the growth front. Free-standing N-polar single-crystal AlN substrates from Asahi-Kasei Corporation were used.[5,18,19] After *ex-situ* cleaning in acetone, isopropyl alcohol and de-ionized water (each for 10 min), diced $7 \times 7\ \text{mm}^2$ AlN substrates were mounted in indium-free holders, loaded into the MBE system and outgassed at 200 °C overnight for 7 h. Before the growth of epi-layers, 100 cycles of *in situ* Al-assisted surface cleaning were performed in the MBE growth chamber to remove the native oxides and other chemical impurities from the N-polar AlN substrate surface and to ensure that the overgrown layers by MBE maintain N-polarity and not flip to metal-polarity.[17] Details about the Al-assisted cleaning process can be found in our previous work.[17,19,20]

After the Al-assisted cleaning, a 500 nm homoepitaxial AlN layer was grown under optimized Al-rich growth condition.[19,20] The excess Al droplets were *in situ* desorbed at an elevated temperature of ∼1200 °C before cooling down the substrate to ∼900 °C for the deposition of a 40 nm undoped $Al_{0.85}Ga_{0.15}N$ layer. After that, for the GaN channel sample ($x = 0$), a 8 nm GaN layer was deposited at a lower substrate temperature of ∼810 °C. A similar growth condition has been used in our previous report.[19] In contrast, for all the AlGaN channel samples ($x > 0$), the 8 nm $Al_xGa_{1-x}N$ channel layers were grown at the same growth temperature as the $Al_{0.85}Ga_{0.15}N$ layers without growth interruption at the heterojunctions. The Al compositions in the $Al_xGa_{1-x}N$ layers were controlled via Al cell temperature. All the AlGaN (and GaN) layers were grown under metal-rich growth conditions and the substrates were held at the growth temperatures for long enough after growth to *in situ* desorb excess Ga droplets before cooling down to room temperature.

The purpose of inserting an $Al_{0.85}Ga_{0.85}N$ "impurity blocking" layer between AlN and the top $Al_xGa_{1-x}N$ layers is to boost 2DEG mobility by blocking unwanted impurities such as silicon "floating" on the growth front of the AlN under the Al-rich growth condition from reaching the top heterojunction where the 2DEG is desired.[18,19,21,22]

Figure 1(b) shows the symmetric $2\theta/\omega$ x-ray diffraction (XRD) scans of the five samples shown in Fig. 1(a) measured using a PANalytical Empyrean setup at 45 kV and 40 mA with Cu Kα1 radiation (1.5406 Å). The observation of thickness fringes indicates abrupt hetero-interfaces. As x increases, the satellites/fringes are resolved more clearly due to the better lattice match to the substrate. Moreover, good agreement between the measured XRD spectra and the simulations (not shown) based on the layer structures in Fig. 1(a) confirm the realization of the targeted structures. Reciprocal space maps (RSMs) around the asymmetric (105) diffraction peaks of GaN,

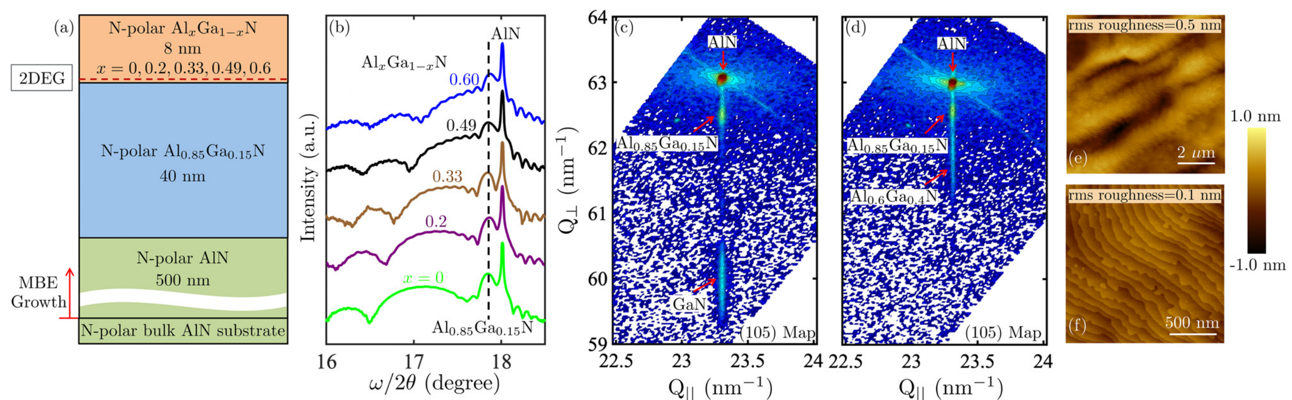

FIG. 1. (a) Schematic of the epitaxial layer structures in this study. (b) Symmetric $2\theta/\omega$ XRD scans across the (002) diffractions with various Al contents. [(c) and (d)] RSMs across the asymmetric (105) diffractions taken from the samples with (c) $x = 0$ and (d) $x = 0.6$. (e) 10×10 and (f) $2 \times 2\ \mu\text{m}^2$ AFM micrographs of the as-grown surface with $x = 0.49$, showing a smooth surface with parallel atomic steps.

Downloaded from http://pubs.aip.org/aip/apl/article-pdf/doi/10.1063/5.0145826/17813233/212106_1_5.0145826.pdf

Published under an exclusive license by AIP Publishing

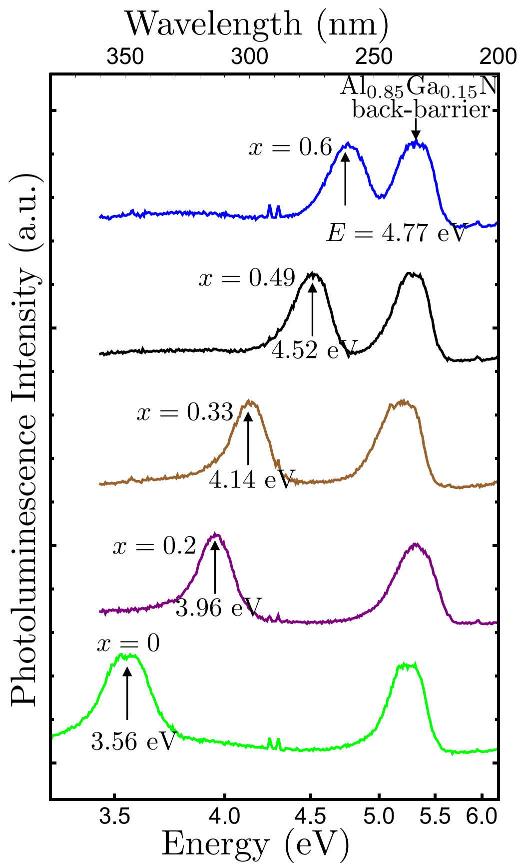

FIG. 2. Photoluminescence spectra of N-polar $Al_xGa_{1-x}N/Al_{0.85}Ga_{0.15}N$ heterostructures with varying Al composition x of the top AlGaN channel layer at $T = 300$ K, showing photon emission from all the samples.

AlGaN and AlN were performed to quantify the strain of the AlGaN (and GaN) layers. All the AlGaN and GaN layers in this study are found to be fully strained to the underlying AlN. Figures 1(c) and 1(d) show the representative RSM scans from the samples with $x = 0$ and $x = 0.6$, respectively. Quantification of strain in the GaN and AlGaN layers is important for understanding the transport properties since strain affects the piezoelectric polarization and hence the 2DEG density.

The surface morphologies of the samples were examined using atomic force microscopy (AFM) in an Asylum Research Cypher ES setup. Figures 1(e) and 1(f) show the as-grown surface morphology with $x = 0.49$ as an example. Smooth surface free of spiral hillocks with a low root mean square (rms) roughness of 0.5 nm was measured in a 10×10 μm^2 area [Fig. 1(e)]. The zoomed in 2×2 μm^2 scan shown in Fig. 1(f) reveals parallel atomic steps, suggesting a step-flow growth mode. Similar surface morphologies with sub-nanometer rms roughness in a 10×10 μm^2 scan and parallel atomic steps were also observed from the other samples. No clear correlation between the surface roughness and Al composition was observed.

Figure 2 shows the 300 K photoluminescence (PL) spectra of the five samples. All the samples were excited by a 193 nm ArF excimer laser from the top. Near band edge PL emission from the top AlGaN channel layer is observed for all five samples. The top AlGaN layer PL peaks at 348 nm (3.56 eV), 312 nm (3.96 eV), 300 nm (4.14 eV), 274 nm (4.52 eV), and 260 nm (4.77 eV) for the GaN, $Al_{0.2}Ga_{0.8}N$, $Al_{0.33}Ga_{0.67}N$, $Al_{0.49}Ga_{0.51}N$, and $Al_{0.6}Ga_{0.4}N$ channel samples, respectively. The PL peak blue-shifts when the Al composition x of the channel increases, providing a direct signature of the increasing bandgap of the channel. It is noted that the apparent optical bandgap of the AlGaN channel measured by PL could differ from the bulk bandgap due to energy quantization, quantum-confined Stark effect (QCSE), and strain. It is interesting to note that photon emission is also observed from the wider bandgap $Al_{0.85}Ga_{0.15}N$ back-barrier at $\sim$234 nm (5.3 eV) from all the samples. A detailed analysis of the PL spectra is not attempted here and is proposed for future work.

Hall-effect measurements were performed on the samples using soldered corner indium contacts to the N-polar AlGaN channel 2DEGs. The results are summarized in Table I, together with the energy bandgap obtained from PL. All samples, with the exception of the one with $Al_{0.6}Ga_{0.4}N$ channel, displayed measurable 2DEGs down to cryogenic temperatures as expected due to their polarization-induced origin. Figure 3(a) shows the simulated energy band diagrams using a self-consistent Schrödinger–Poisson solver for the channel Al content $x = 0, 0.33, 0.6$ with a surface barrier height $q\phi_B$ of 0.3 eV (as has been reported for N-polar GaN[19,23]) and a zero electric field deep inside the bulk AlN as boundary conditions. As shown in Fig. 3(b), high-density 2DEGs are induced at the top $Al_xGa_{1-x}N/Al_{0.85}Ga_{0.15}N$ interfaces. The secondary channel at the bottom interface has been found to show no measurable conductivity.[19] The reason behind the high resistivity of the secondary channel is still under investigation at this point. One possible explanation is the localization in deep levels.

Downloaded from http://pubs.aip.org/aip/apl/article-pdf/doi/10.1063/5.0145826/17813233/212106_1_5.0145826.pdf

TABLE I. Structural details of the N-polar $Al_xGa_{1-x}N/Al_{0.85}Ga_{0.15}N$ HEMT heterostructures studied in this work, with the corresponding bandgap of the AlGaN channel measured via PL and their 2DEG densities n_s, mobilities μ measured via Hall-effect at 300 and 77 K. Sheet resistance R_s of $>10^3$ kΩ/sq. indicates resistive samples in which the transport could not be extracted using Hall effect measurements. The surface barrier heights $q\phi_b$ are extracted by fitting the simulation with the measured 2DEG densities.

Channel layer	Energy bandgap from PL (eV)	n_s^{300K} (10^{13}/cm^2)	μ^{300K} [cm^2/(V s)]	R_s^{300K} (kΩ/sq.)	n_s^{77K} (10^{13}/cm^2)	μ^{77K} [cm^2/(V s)]	R_s^{77K} (kΩ/sq.)	$q\phi_b$ (eV)
GaN	3.56	3.8	653	0.25	3.3	1430	0.13	0.4
$Al_{0.2}Ga_{0.8}N$	3.96	3.0	156	1.33	2.8	192	1.16	0.5
$Al_{0.33}Ga_{0.67}N$	4.14	2.0	101	3.09	1.7	105	3.5	1.0
$Al_{0.49}Ga_{0.51}N$	4.52	0.76	43	19.12	0.69	39	23.22	1.7
$Al_{0.6}Ga_{0.4}N$	4.77	...	...	$>10^3$	...	...	$>10^3$	...

Published under an exclusive license by AIP Publishing

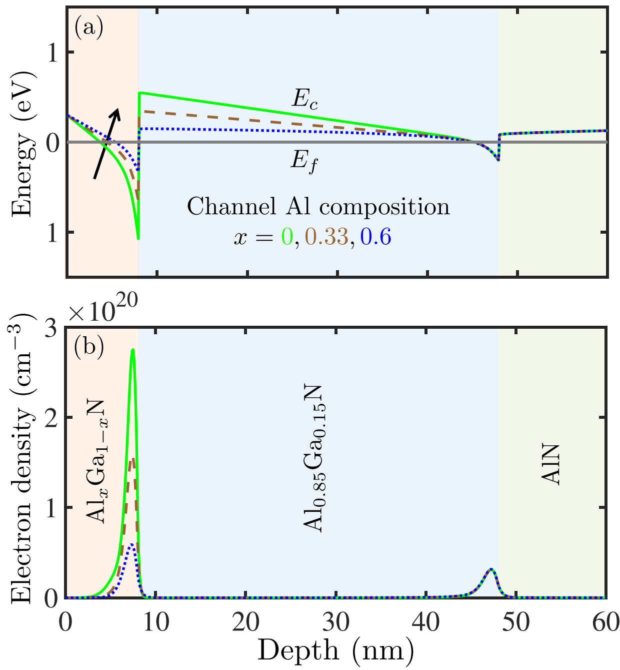

FIG. 3. (a) Simulated energy band diagrams for three different Al compositions $x = 0$ (green), 0.33 (brown), and 0.6 (blue) with a surface barrier height $q\phi_B \sim 0.3$ eV. (b) Simulated electron densities confirm the presence of high-density 2DEGs at $Al_xGa_{1-x}N/Al_{0.85}Ga_{0.15}N$ interfaces. The secondary channel at the bottom interface does not show measurable conductivity.[19]

The following discussion will focus only on the 2DEGs at the top heterointerface.

With increasing Al content in the channel, the conduction band edge E_c at the top heterointerface moves up toward the Fermi level [Fig. 3(a)] and the 2DEG density decreases [Fig. 3(b)]. While the energy band diagram simulation with a fixed surface barrier height of 0.3 eV *qualitatively* explains the diminishing trend of 2DEG density with increasing Al content in the channel, it predicts a high density ($n_s > 1\times 10^{13}/\text{cm}^2$) 2DEG at $Al_{0.6}Ga_{0.4}N/Al_{0.85}Ga_{0.15}N$, which contrasts the absence of any measurable conductivity in that sample. Meanwhile, it also predicts a 2DEG density of $n_s > 1.7\times 10^{13}/\text{cm}^2$ for $x = 0.49$, which is more than a factor of 2 overestimate of the measured 2DEG density of $0.76 \times 10^{13}/\text{cm}^2$. This is further illustrated in Fig. 4(a): although the measured 300 K 2DEG density for $x \leq 0.2$ agrees reasonably well with the simulation with $q\phi_B = 0.3$ eV, the measured 2DEG density drops much faster than is predicted for $x \geq 0.33$, which indicates a substantial deviation from fixed surface barrier height $q\phi_B = 0.3$ eV for high Al content AlGaN channel. For example, a surface barrier height of $\sim$2 eV is expected for $x = 0.49$ from Fig. 4(a). The surface barrier height $q\phi_B$ that matches the simulated 2DEG density at $Al_xGa_{1-x}N/Al_{0.85}Ga_{0.15}N$ interface with the measured value at 300 K for each sample is listed in the last column of Table I. The increase in surface barrier height with increasing Al composition has been reported for metal-polar AlGaN using x-ray photoelectron spectroscopy (XPS) technique.[24] It is interesting that a similar trend is also observed for N-polar AlGaN.

Figure 4(b) shows the measured 77 (filled symbols) and 300 K (hollow symbols) Hall effect mobilities as a function of Al composition x. The 2DEG mobility degrades monotonically with increasing Al

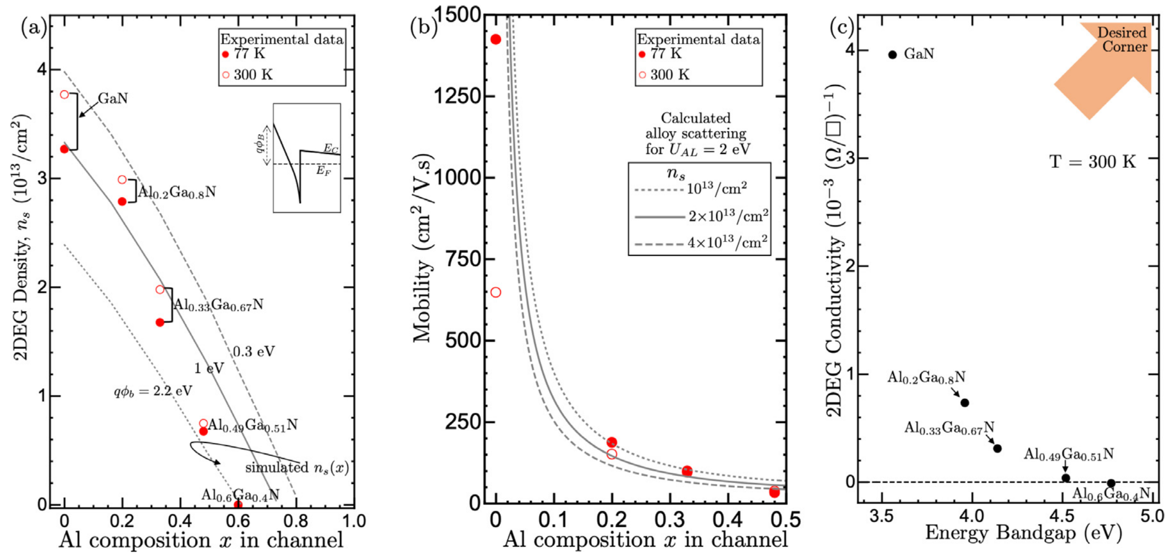

FIG. 4. (a) Measured 2DEG Hall densities at 77 K (filled circles) and 300 K (hollow circles) as a function of Al composition x in the AlGaN channel layer for different samples. The simulated 2DEG densities (gray lines) are also plotted as a function of Al composition for different surface barrier heights $q\phi_B$ (inset) and show good agreement with the experimental data. (b) 77 K (filled circles) and 300 K (hollow circles) electron mobilities as a function of Al composition x in the AlGaN 2DEG channel. The gray curves show the calculated alloy scattering mobilities for different carrier densities n_s for the same alloy scattering potential $U_{AL} = 2$ eV which confirms that the major scattering mechanism in high Al composition AlGaN channel 2DEGs is alloy scattering. (c) Sheet conductivity vs energy bandgap from PL for various Al compositions. High conductivity is desired for high current, whereas large energy bandgap is preferred for high breakdown voltage.

Downloaded from http://pubs.aip.org/aip/apl/article-pdf/doi/10.1063/5.0145826/17813233/212106_1_5.0145826.pdf

Published under an exclusive license by AIP Publishing

composition x, from $\mu > 1400\,\text{cm}^2/\text{V s}$ for $x = 0$ to $\mu < 50\,\text{cm}^2/\text{V s}$ for $x = 0.49$ at 77 K. It is apparent that the 77 K mobility shows $>2\times$ increase compared to its 300 K value for the GaN channel ($x = 0$) as expected due to freeze out of phonon scattering. A slight increase in low-temperature mobility is also observed for $Al_{0.2}Ga_{0.8}N$ channel compared to its room-temperature value, whereas the change is almost negligible for $Al_{0.33}Ga_{0.67}N$ and $Al_{0.49}Ga_{0.51}N$ channel 2DEGs. Both the decrease in 2DEG mobility with increasing Al content and the negligible temperature dependence in high Al content AlGaN channels can be explained by alloy disorder scattering, which is temperature independent.[25] The alloy scattering limited mobility is known to follow a U-shaped curve as a function of alloy composition x due to the $1/\{x(1-x)\}$ dependence.[26] As a result, within the alloy composition range studied in this work, an increase in Al content x should lead to a decrease in 2DEG mobility. The lines in Fig. 4(b) plot the alloy scattering limited 2DEG mobility as a function of Al content for given 2DEG densities ranging from 1×10^{13} to $4 \times 10^{13}/\text{cm}^2$. An alloy scattering potential $U_{AL} = 2$ eV gives a good fit to the experimental data and falls in the typical range of U_{AL} (between 1.3 and 2.2 eV) reported for metal-polar AlGaN.[9,27–29] The nearly temperature-independent 2DEG mobilities in high Al content AlGaN channels are attractive for applications that require stable operation at high and variable temperatures.

As mentioned earlier, the N-polar AlGaN/AlN 2DEGs observed here can be the enablers for N-polar AlGaN channel HEMTs on AlN. These devices are expected to bring compelling advantages over their GaN channel counterparts, which have been demonstrated recently with promising DC and RF characteristics such as an on-current of 2.6 A/mm and a maximum oscillation frequency (f_{max}) of 100 GHz.[30,31] In addition, thanks to the absence of top barriers, exploiting AlGaN channel in a N-polar structure has the potential to overcome the issue with poor electrical contacts, which has remained one of the major challenges faced by metal-polar AlGaN transistors.[3,4,32] For RF HEMTs, sheet conductivity σ and energy bandgap of the channel E_g are key predictors of their performances. This is because a high σ is desired to achieve large on-currents and low access resistances, whereas a large E_g is also desired for a high critical electric field in the 2DEG channel.

To better illustrate the potential of these 2DEGs for RF and power applications, the experimentally measured room temperature Hall sheet conductivity σ as a function of the experimentally measured energy bandgap from PL for the five samples in the present study are plotted in Fig. 4(c). σ drops rapidly as the E_g of the channel increases. This presents a trade-off between σ and E_g for use in AlGaN channel HEMTs. On the other hand, the absence of as-grown 2DEG in $Al_{0.6}Ga_{0.4}N/Al_{0.85}Ga_{0.15}N$ heterostructure can be advantageous for applications where normally off operation is desired such as power switching and energy conversion,[33] although clever strategies such as selective-area ion implantation of Si need to be employed to lower the access resistance in such devices. Therefore, this study provides useful experimental data for heterostructure design and device engineering toward N-polar AlGaN channel HEMTs for next-generation RF and power electronics.

In summary, a systematic study of the structural, optical, and electronic transport properties of N-polar $Al_xGa_{1-x}N/Al_{0.85}Ga_{0.15}N$ heterostructures with AlGaN channel composition ranging from $x = 0$ to $x = 0.6$, grown using MBE on bulk AlN, is reported in this work. Photoluminescence spectra show that the bandgap of the $Al_xGa_{1-x}N$ channel increases with x, ranging from 3.56 to 4.77 eV. Polarization-induced 2DEGs are observed with 2DEG densities varying from $\sim 3.8 \times 10^{13}/\text{cm}^2$ in the GaN channel to no measurable 2DEG in an $Al_{0.6}Ga_{0.4}N$ channel of thickness 8 nm. Temperature-independent alloy scattering is found to be the major scattering mechanism for high Al content ($x > 0.3$) AlGaN channel 2DEGs. These results lay the groundwork for the design of N-polar AlGaN channel HEMTs on AlN for the high-frequency, high-power, and high-temperature performance.

The authors thank Len van Deurzen for helpful discussions. The authors at Cornell University acknowledge the financial support from Asahi Kasei (materials growth), the Cornell Center for Materials Research (CCMR) (optical characterization)—a NSF MRSEC program (No. DMR-1719875); ULTRA (transport modeling), an Energy Frontier Research Center funded by the U.S. Department of Energy (DOE), Office of Science, Basic Energy Sciences (BES), under Award No. DE-SC0021230, AFOSR Grant No. FA9550-20-1-0148 (structural characterization), and ARO Grant No. W911NF2220177 (energy diagram modeling). This work uses the CESI Shared Facilities partly sponsored by NSF No. MRI DMR-1631282 and Kavli Institute at Cornell (KIC).

AUTHOR DECLARATIONS

Conflict of Interest

The authors have no conflicts to disclose.

Author Contributions

Z. Zhang and J. Singhal contributed equally to this work.

Zexuan Zhang: Conceptualization (lead); Data curation (lead); Formal analysis (lead); Investigation (lead); Methodology (lead); Validation (lead); Writing – original draft (lead); Writing – review & editing (lead). **Jashan Singhal:** Conceptualization (lead); Data curation (lead); Formal analysis (lead); Investigation (lead); Methodology (lead); Validation (lead); Writing – original draft (lead); Writing – review & editing (lead). **Shivali Agrawal:** Investigation (supporting); Methodology (supporting). **Eungkyun Kim:** Investigation (supporting); Writing – review & editing (supporting). **Vladimir Protasenko:** Investigation (supporting); Methodology (supporting). **Masato Toita:** Funding acquisition (equal); Project administration (equal); Writing – review & editing (supporting). **Huili Grace Xing:** Conceptualization (equal); Funding acquisition (equal); Project administration (equal); Resources (equal); Supervision (equal); Writing – review & editing (equal). **Debdeep Jena:** Conceptualization (equal); Funding acquisition (equal); Project administration (equal); Resources (equal); Supervision (equal); Writing – review & editing (equal).

DATA AVAILABILITY

The data that support the findings of this study are available from the corresponding author upon reasonable request.

REFERENCES

[1] J. Tsao, S. Chowdhury, M. Hollis, D. Jena, N. Johnson, K. Jones, R. Kaplar, S. Rajan, C. Van de Walle, E. Bellotti *et al.*, Adv. Electron. Mater. **4**, 1600501 (2018).

Downloaded from http://pubs.aip.org/aip/apl/article-pdf/doi/10.1063/5.0145826/17813233/212106_1_5.0145826.pdf

Published under an exclusive license by AIP Publishing

[2]M. Higashiwaki, R. Kaplar, J. Pernot, and H. Zhao, Appl. Phys. Lett. **118**, 200401 (2021).
[3]I. Abid, J. Mehta, Y. Cordier, J. Derluyn, S. Degroote, H. Miyake, and F. Medjdoub, Electronics **10**, 635 (2021).
[4]R. Maeda, K. Ueno, A. Kobayashi, and H. Fujioka, Appl. Phys. Express **15**, 031002 (2022).
[5]Z. Zhang, M. Kushimoto, T. Sakai, N. Sugiyama, L. J. Schowalter, C. Sasaoka, and H. Amano, Appl. Phys. Express **12**, 124003 (2019).
[6]L. van Deurzen, R. Page, V. Protasenko, K. Nomoto, H. Xing, and D. Jena, AIP Adv. **12**, 035023 (2022).
[7]J. Simon, V. Protasenko, C. Lian, H. Xing, and D. Jena, Science **327**, 60 (2010).
[8]R. Dalmau and B. Moody, ECS Trans. **86**, 31 (2018).
[9]J. Singhal, R. Chaudhuri, A. Hickman, V. Protasenko, H. G. Xing, and D. Jena, APL Mater. **10**, 111120 (2022).
[10]D. Khachariya, S. Mita, P. Reddy, S. Dangi, J. H. Dycus, P. Bagheri, M. H. Breckenridge, R. Sengupta, S. Rathkanthiwar, R. Kirste *et al.*, Appl. Phys. Lett. **120**, 172106 (2022).
[11]J. Lemettinen, N. Chowdhury, H. Okumura, I. Kim, S. Suihkonen, and T. Palacios, IEEE Electron Device Lett. **40**, 1245 (2019).
[12]L. You, W. Matsumura, K. Ataka, S. Matsuda, D. Inahara, K. Hanasaku, R. Okuno, T. Kowaki, Y. Yao, Y. Ishikawa *et al.*, Jpn. J. Appl. Phys. **62**, SA1018 (2023).
[13]A. Kaminska, K. Koronski, P. Strak, A. Wierzbicka, M. Sobanska, K. Klosek, D. V. Nechaev, V. Pankratov, K. Chernenko, S. Krukowski *et al.*, Appl. Phys. Lett. **117**, 232101 (2020).
[14]D. Jena, A. C. Gossard, and U. K. Mishra, Appl. Phys. Lett. **76**, 1707 (2000).
[15]S. Besendörfer, E. Meissner, F. Medjdoub, J. Derluyn, J. Friedrich, and T. Erlbacher, Sci. Rep. **10**, 17252 (2020).
[16]D. Li, H. Chen, H. Yu, H. Jia, Q. Huang, and J. Zhou, J. Appl. Phys. **96**, 1111 (2004).
[17]Z. Zhang, Y. Hayashi, T. Tohei, A. Sakai, V. Protasenko, J. Singhal, H. Miyake, H. G. Xing, D. Jena, and Y. Cho, Sci. Adv. **8**, eabo6408 (2022).
[18]Z. Zhang, J. Encomendero, R. Chaudhuri, Y. Cho, V. Protasenko, K. Nomoto, K. Lee, M. Toita, H. G. Xing, and D. Jena, Appl. Phys. Lett. **119**, 162104 (2021).
[19]Z. Zhang, J. Encomendero, E. Kim, J. Singhal, Y. Cho, K. Nomoto, M. Toita, H. G. Xing, and D. Jena, Appl. Phys. Lett. **121**, 082107 (2022).
[20]J. Singhal, J. Encomendero, Y. Cho, L. van Deurzen, Z. Zhang, K. Nomoto, M. Toita, H. G. Xing, and D. Jena, AIP Adv. **12**, 095314 (2022).
[21]R. Chaudhuri, Z. Chen, D. A. Muller, H. G. Xing, and D. Jena, J. Appl. Phys. **130**, 025703 (2021).
[22]R. Chaudhuri, Z. Zhang, H. G. Xing, and D. Jena, Adv. Electron. Mater. **8**, 2101120 (2022).
[23]Ł. Janicki, J. Misiewicz, M. Siekacz, H. Turski, J. Moneta, S. Gorantla, C. Skierbiszewski, and R. Kudrawiec, Sens. Actuators, B **281**, 561 (2019).
[24]P. Reddy, I. Bryan, Z. Bryan, J. Tweedie, S. Washiyama, R. Kirste, S. Mita, R. Collazo, and Z. Sitar, Appl. Phys. Lett. **107**, 091603 (2015).
[25]G. Bastard, *Wave Mechanics Applied to Semiconductor Heterostructures* (John Wiley and Sons Inc., New York, NY USA, 1990).
[26]M. Miyoshi, S. Fujita, and T. Egawa, Appl. Phys. Express **8**, 051003 (2015).
[27]D. Jena, S. Heikman, J. S. Speck, A. Gossard, U. K. Mishra, A. Link, and O. Ambacher, Phys. Rev. B **67**, 153306 (2003).
[28]J. Simon, A. Wang, H. Xing, S. Rajan, and D. Jena, Appl. Phys. Lett. **88**, 042109 (2006).
[29]N. Pant, Z. Deng, and E. Kioupakis, Appl. Phys. Lett. **117**, 242105 (2020).
[30]E. Kim, Z. Zhang, J. Encomendero, J. Singhal, K. Nomoto, A. Hickman, C. Wang, P. Fay, M. Toita, D. Jena *et al.*, Appl. Phys. Lett. **122**, 092104 (2023).
[31]E. Kim, Z. Zhang, J. Singhal, K. Nomoto, A. Hickman, M. Toita, D. Jena, and H. G. Xing, in *2022 Device Research Conference (DRC)* (IEEE, 2022), pp. 1–2.
[32]R. Kaplar, A. A. Allerman, A. Armstrong, M. H. Crawford, J. R. Dickerson, A. J. Fischer, A. Baca, and E. Douglas, ECS J. Solid State Sci. Technol. **6**, Q3061 (2017).
[33]S. Bajaj, T.-H. Hung, F. Akyol, D. Nath, and S. Rajan, Appl. Phys. Lett. **105**, 263503 (2014).

Downloaded from http://pubs.aip.org/aip/apl/article-pdf/doi/10.1063/5.0145826/17813233/212106_1_5.0145826.pdf

Published under an exclusive license by AIP Publishing